ELSEVIER

Thin Solid Films 402 (2002) 71–78

thin solid films

www.elsevier.com/locate/tsf

Structural and electrical studies on highly conducting spray deposited fluorine and antimony doped SnO_2 thin films from $SnCl_2$ precursor

B. Thangaraju*

Department of Physics, Bharathidasan University, Trichy 620 024, Tamil Nadu, India

Received 18 August 2000; received in revised form 10 May 2001; accepted 21 September 2001

Abstract

Tin oxide thin films doped with fluorine, antimony and both have been prepared by spray pyrolysis from $SnCl_2$ precursor. The respective deposition temperatures of SnO_2:F, SnO_2:Sb and SnO_2:(F+Sb) are 400 °C, 350 °C and 375 °C. The as-prepared films are polycrystalline with a tetragonal crystal structure. The lattice parameter values are not changed by the addition of dopants. The films are preferentially oriented along the (200) direction. The grain sizes vary between 200 and 650 Å. The films have moderate optical transmission (up to 70% at 800 nm) and the calculated reflectivity in the infra-red region is in the range of 88–95%. The figure of merit (ϕ) values of SnO_2:F and SnO_2:Sb samples are 2.5×10^{-3} $(\Omega)^{-1}$ and 1.4×10^{-4} $(\Omega)^{-1}$, respectively. The films are heavily doped, degenerate and exhibit n-type electrical conductivity. The lowest sheet resistance (R_{sh}) of 5.65 $\Omega/\square$ obtained for a SnO_2:F sample, is even lower than the values reported for the spray deposited tin oxide thin films prepared from $SnCl_2$ precursor. The resistivity (ρ) and mobility (μ) are in the range of 10^{-4}–10^{-3} Ω-cm and 7–17.2 $cm^2\ V^{-1}\ s^{-1}$. The electron density lies between 1.3×10^{20} and 13.2×10^{20} cm^{-3}. A thorough electrical investigation reveals that the film's conductivity depends only on carrier concentration. It is found that ionised impurity scattering is the dominant mechanism, which limits the mobility of the carriers.

Keywords: Electrical properties and measurements; Pyrolysis; Tin oxide; X-Ray diffraction

1. Introduction

An important application of thin film technology from the point of view of global energy crunch is solar cell, which converts the energy of the solar radiation into useful electrical energy. In recent years there has been a growing interest in the use of transparent conducting oxide thin films as conducting solar window materials in thin film solar cells [1], heat reflectors for advanced glazing in solar applications [2,3] and as various gas sensors [4–7]. Tin oxide is the first transparent conductor to have received significant commercialisation [8]. Among the different transparent conductive oxides, SnO_2 films doped with fluorine or antimony seem to be the most appropriate for use in solar cells, owing to its low electrical resistivity and high optical transmittance. SnO_2 is chemically inert, mechanically hard and can resist high temperature. Many excellent reviews of transparent conductive oxides are available [9–14]. SnO_2 either doped or undoped can be synthesised by numerous techniques such as thermal evaporation [4], sputtering [4,15–22] chemical vapour deposition [23,24], metallo-organic chemical vapour deposition (MOCVD) [5], sol–gel dip coating [25], painting [26], spray pyrolysis [2,9,27–45], hydrothermal method [46] and pyrosol deposition [47,48]. Among the various deposition techniques the spray pyrolysis is the well suited for the preparation of doped tin oxide thin films because of its simple and inexpensive experimental arrangement, ease of adding various doping material, reproducibility, high growth rate and mass production

* Department of Physics, Indian Institute of Science, Bangalore 560 012, India. Tel.: +91-80-3092716; fax: +91-80-3602602, 3600683, 3600085.

E-mail address: raju@physics.iisc.ernet.in (B. Thangaraju).

0040-6090/02/$ - see front matter
PII: S0040-6090(01)01667-4

capability for uniform large area coatings, which are desirable for industrial and solar cell applications.

Stoichiometric SnO_2 is a perfect insulator but the material becomes semi-metallic when fabricated by the spraying method [27]. Spray pyrolysis basically comes under the category of a chemical solution deposition technique [49]. The fine mist of very small droplets of the aqueous solution containing the desired species is sprayed onto a preheated substrate. The thermal decomposition takes place on the hot substrate surface giving rise to a continuous film. The tin oxide films prepared by the spray pyrolysis using $SnCl_4$ based solution as the source of tin is common [2,9,35–47] though other precursors are also reported [12,13]. Very few reports are available using $SnCl_2$ as a precursor of tin for tin oxide thin film [25,28,42,47,50]. The author has already reported the preparation and characterisation of $PbSnS_2$, SnS and SnS_2 thin films by the spray pyrolysis using $SnCl_2$ as a source material for tin [51,52]. The advantages of the $SnCl_2$ are that is cheaper than $SnCl_4$ and can be produced easily in a laboratory [42]. The prime aim of this work is to produce highly conducting F and Sb doped tin oxide thin films from $SnCl_2$ precursor solution and to investigate their structural and electrical properties.

2. Experimental details

A laboratory built double nozzle glass sprayer is used to prepare the thin film samples of the present study. The schematic diagram of the experimental set-up and other details have been reported elsewhere [53,54]. A mixture of 15 g of $SnCl_2 \cdot 2H_2O$ salt and 5 ml of HCl is heated slightly. This mixture is diluted by adding methanol and the diluted solution is made up to 50 ml by adding triply distilled water. This forms the basic solution of the spray liquid. Ammonium fluoride diluted with water is added to this solution in proper proportions to effect fluorine doping. Antimony doping is done with $SbCl_3$ dissolved in methanol.

Filtered compressed air is used as carrier gas and the flow rate is 7 l/min at a pressure of 7.59×10^4 N m^{-2}. The solution flux is kept at 4 ml min^{-1}. The normalised distance between the spray nozzle and the substrate is 35 cm. Optical microslide glass plates with an effective area of 7.5×2.5 cm are used as substrates. The substrates are cleaned with organic solvents and rinsed with triply distilled water before spraying. The spray liquid, prepared from the basic solution with different concentrations of NH_4F or $SbCl_3$ or both, is then sprayed onto the hot substrates where pyrolysis and film deposition occurs. The normalised deposition temperatures are 400 °C, 350 °C and 375 °C for fluorine, antimony and (F+Sb) doped films, respectively. At a temperature lower than these optimum values a yellowish coloration of the sample appears due to the unconverted precursor and for higher temperatures a white fog is found due to the excess of tin.

The spray time is maintained at 1 s. To avoid excess cooling of the substrates a 2-min waiting time is allowed between successive spraying applications. Uniform coating is achieved by rotating the substrate through a predetermined angle in its plane after each application. The F, Sb and (F+Sb) dopant ratio are varied over a wide range and all other experimental parameters are fixed at their optimum values. The $[NH_4F]/[SnCl_2]$ ratio by weight percentage in the spray liquid is kept at values of 4, 6, 8, 10 and 15, the $[SbCl_3]/[SnCl_2]$ ratio at 0.2, 0.4, 0.6, 1 and 2 and the $[NH_4F + SbCl_3]/[SnCl_2]$ ratio at 7.5+1, 8+1, 12+1, 10+0.2, 10+0.5 and 15+0.5. Reproducibility is achieved by controlling the deposition parameters. In all, more than 50 films were deposited for each concentration, fixing the thickness at a constant value. The as-prepared films were structurally, electrically and electro-optically characterised. All the measurements were carried out on 1-μm-thick films. The thickness of the film was measured by a conventional mass method [38,52–55].

The structural properties of the films were studied by computer controlled RIGAKU, X-ray diffractometer using CuK_α (1.5418 Å) radiation. The scanning angle 2θ was varied from 10 to 90° in step of 0.02° and the scanning speed was fixed at 2° min^{-1}.

The electrical resistivity and Hall mobility were measured using the standard van der Pauw four probe method [56]. Colloidal silver paint was used as the ohmic contact. The variation of resistivity with temperature was measured from 30 to 200 °C. The n-type electrical conductivity of the films was confirmed by the Hall measurement. The Hall probe experimental arrangement and the measurement details can be found in Thangaraju [57]. Optical transmittance measurements were carried out using a Hitachi model 3400 UV-VIS-NIR, double beam spectrophotometer.

3. Results and discussion

3.1. Structural analysis

Since changes in the structural properties of SnO_2 films can be correlated with the variations of the electrical and optical properties, XRD measurements were made to determine the phase, crystallographic structure and the grain size of the crystallites. Typical X-ray diffraction spectra recorded on SnO_2:F ($[NH_4F]/[SnCl_2] = 10$ wt.%), SnO_2:Sb ($[SbCl_3]/[SnCl_2] = 0.4$ wt.%) and SnO_2:(F+Sb) ($[NH_4F + SbCl_3]/[SnCl_2] = 10+0.5$ wt.%) films are shown in Fig. 1. All the diffractograms contain the characteristic SnO_2 peaks only. Other phases (SnO, Sn_2O_3 or SnF_2), as reported to occur in SnO_2 films [23,58,59] are not observed in the deposited layers. The (200) peak is the strongest

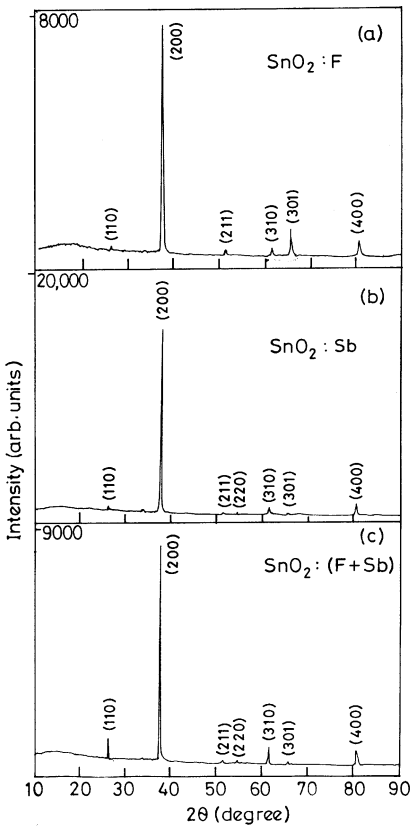

Fig. 1. X-Ray diffraction spectra of (a) SnO_2:F ($[NH_4F]/[SnCl_2]=10$ wt.%); (b) SnO_2:Sb ($[SbCl_3]/[SnCl_2]=0.4$ wt.%); and (c) SnO_2:(F+Sb)$[NH_4F]/[SnCl_2]+[SbCl_3]/[SnCl_2]=[10]+[0.5]$ wt.%) thin films.

peak observed for all the films. Other peaks observed are (110), (211), (220), (310), (301) and (400). The addition of dopants does not affect the preferred (200) orientational growth of the films. One significant difference is the intensity of this peak. Antimony doping leads to the peak intensity higher than the other dopants.

The most striking feature from the XRD results is that the films prepared for the present study are highly oriented with the (200) plane parallel to the substrate. It was, however, reported by Grodillo et al. [42] that doped and undoped SnO_2 films prepared by spray pyrolysis from $SnCl_2$ precursor present a preferential growth along the (110) direction. The precursor chemistry and growth rate have been analysed by them for the deposition of SnO_2 films from $SnCl_4$ and $SnCl_2$. The exact reasons for this difference may be sought in the differences in the preparation of starting solutions. Smith et al. [47] have analysed the preparation of SnO_2 films, with and without addition of HCl in $SnCl_2{\cdot}2H_2O$ solution. It is found that without addition of HCl in the starting solution, the films preferred orientation is (110), whereas the HCl (>0.2 mol l^{-1}) added with the starting solution, the films are highly oriented in (200) direction. This can be attributed to the

Table 1
XRD data of doped SnO_2 thin films

Standard[a]		Observed (Å)		
d (Å)	(*hkl*)	F	Sb	(F+Sb)
3.351	110	–	3.373	3.371
2.369	200	2.398	2.386	2.384
1.765	211	1.776	1.776	1.772
1.675	220	–	1.684	1.683
1.498	310	1.508	1.508	1.507
1.415	301	1.425	1.425	1.422
1.184	400	1.192	1.192	1.192

The spray solution dopant wt. ratios correspond to $[NH_4F]/[SnCl_2]=10$ wt.%, $[SbCl_3]/[SnCl_2]=0.4$ wt.% and $[NH_4F]/[SnCl_2]+[SbCl_3]/[SnCl_2]=[10]+[0.5]$ wt.%.

[a] JCPDS card no: 21-1252.

different formation of the molecules in the starting solution. In $SnCl_2{\cdot}2H_2O$ solution, tin based polymer molecule is formed. $SnCl_4$ dissolved in alcohol forms complexes like $SnCl_4{\cdot}2CH_3OH$ [60], which decompose at the pyrolysis temperature to form hydrated SnO_2 on the substrate. The hydrated SnO_2 molecule is formed by yet another way, from $SnCl_2{\cdot}2H_2O+HCl$ solution. $SnCl_2{\cdot}2H_2O$ reacts with HCl to form $HSnCl_3$; this neutral $HSnCl_3$ molecule is unstable and highly reactive [61]. At the pyrolysis temperature, $HSnCl_3$ is thermally decomposed to form the hydrated SnO_2 molecule.

It has been reported from the SEM micrograph analysis that the film morphology of $SnCl_2{\cdot}2H_2O$ with HCl precursor is similar to that obtained with $SnCl_4$ [47]. It is well established now, that SnO_2 films deposited from $SnCl_4$ precursor at temperatures of approximately 400 °C always grow in (200) direction [35,37,39,41–43]. It is therefore not surprising that in the present investigation the films are highly oriented in the (200) direction since they are prepared from the $SnCl_2{\cdot}2H_2O+HCl$ starting solution.

Tin oxide is a tetragonal system. The observed *d* values are presented in Table 1. Standard data taken from literature are included in the table for the purpose of comparison. The lattice parameter values *a* and *c* calculated for these samples are presented in Table 2. It is evident from the table that the lattice parameters are not affected much by the incorporation of the dopants in the films [35]. The grain sizes calculated using Scherrer's formula, vary between 200 and 650 Å. In fluorine doped films the crystallites are comparatively

Table 2
Lattice parameter data of doped SnO_2 thin films

Lattice parameter	Standard[a]	F	Sb	(F+Sb)
a (Å)	4.737	4.761	4.768	4.765
c (Å)	3.187	3.225	3.210	3.194

[a] JCPDS card no: 21-1252.

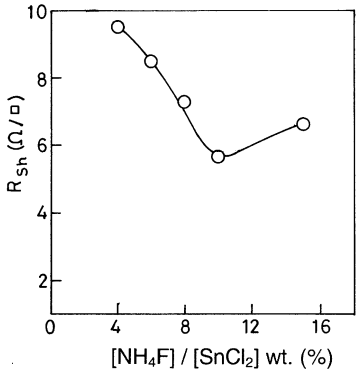

Fig. 2. Variation of sheet resistance with dopant ratio for SnO_2:F thin films.

smaller in size. Antimony doping increases the size of the grains and the combined (F+Sb) doping increases the grain size further.

3.2. Electo-optical studies

Sheet resistance (R_{sh}) is a useful parameter in comparing thin films, particularly those of the same material deposited under similar conditions. The plots of sheet resistance vs. dopant concentration in the spray solution for SnO_2:F (FTO) and SnO_2:Sb (ATO) films are shown in Figs. 2 and 3, respectively. R_{sh} decreases with concentration initially reaches a minimum and increases beyond this particular concentration.

In the fluorine doped tin oxide films, the F^- anion substitutes for an O^{2-} anion in the lattice, creates more free electrons and decreases the value of R_{sh}. The minimum value is obtained at $[NH_4F]/[SnCl_2]=10$ wt.%. Increasing the value of R_{sh} after a specific level of F content probably represents a solubility limit of F in the tin oxide lattice. The excess F atoms do not occupy the proper lattice positions to contribute to the free carrier concentration and at the same time the increasing disorder leads to the increase of the sheet resistance.

When Sb is added to SnO_2, Sb is incorporated into the Sn^{4+} sites of the SnO_2 lattice substitutionally. In ATO samples, Sb is in two different oxidation states namely, Sb^{5+} and Sb^{3+}. During the initial addition of Sb in tin oxide film, the Sb^{5+} substituted on the Sn^{4+} site act as donors and create excess electrons. So the free carrier concentration is higher and consequently the sheet resistance decreases with the addition of Sb up to a certain level. At $[SbCl_3]/[SnCl_2]=0.6$ wt.%, the film reaches the minimum value of sheet resistance. Further addition of Sb introduces the Sb^{3+} sites, which act as acceptors. The Sb^{3+} species would compensate the donor levels, which were created by the Sb^{5+} species, leading to an increase in the R_{sh}.

The minimum value of sheet resistance is 5.65 and 8.1 Ω/□ for FTO and ATO films, respectively. These sheet resistance values agree with the reported films deposited by $SnCl_4$ [28,30–32,36–38,40–42,44,45,47,55]. The R_{sh} of 5.65 Ω/□ is the lowest value among the reported SnO_2 films, prepared from $SnCl_2$ starting solution [28,42,47].

Transparency (T) and conductivity are strongly interrelated and the nature of this interdependence is dictated by the influence of various deposition parameters on the electro-optical properties of the films. For films deposited under optimum conditions, R_{sh} and T depend significantly on the film thickness. In the present study the thickness of the films are approximately 1 μm, which is higher compared to the reported film thickness [28,42,47]; this higher thickness affects the optical transmission. All the films show only moderate transmission. The highest transmittances obtained (at 800 nm) are in FTO samples at $[NH_4F]/[SnCl_2]=6$ wt.% and in ATO samples at $[SbCl_3]/[SnCl_2]=0.2$ wt.% are 70% and 55% respectively. A good criterion to define the quality of highly transparent and conductive thin film is through the introduction of a figure of merit calculated using Haacke's equation $\phi=T^{10}/R_{sh}$ [62]. The figure of merit of FTO and ATO samples are 2.5×10^{-3} $(\Omega)^{-1}$ and 1.4×10^{-4} $(\Omega)^{-1}$, respectively. The FTO film figure of merit is one order higher than the figure of merit of the ATO film. This is quite expected because antimony doping leads to higher R_{sh} values and the appearance of bluish coloration due to the addition of doping leads to the poor transmission [41]. A comparison of electro-optical properties of SnO_2 films prepared by various techniques can be found in reference [33]. The transmittance spectra of the films and the optical investigations will be published elsewhere.

The reflectivity R of the samples is calculated using the relation [33]

$$R=(1+2\varepsilon_0 C_0 R_{sh})^{-2} \quad (1)$$

with $1/\varepsilon_0 C_0=376$ Ω (the free space impedance), which is valid over a wide range in the IR region. The

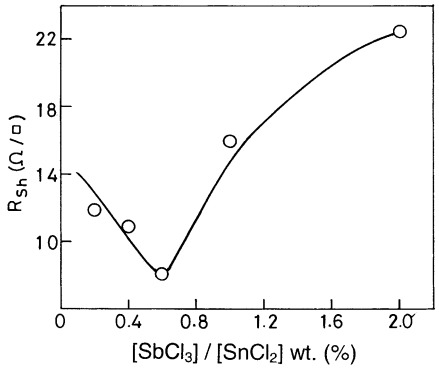

Fig. 3. Variation of sheet resistance with dopant ratio for SnO_2:Sb thin films.

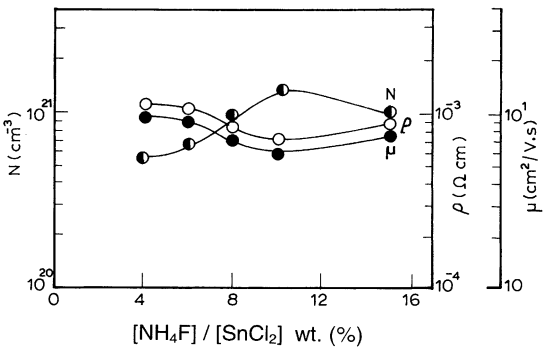

Fig. 4. Variation of Hall mobility (μ), carrier density (*N*) and resistivity (ρ) with dopant weight ratio for SnO_2:F thin films.

calculated *R* values are lying in the range of 88–95%. The high *R* values of the samples, along with high *T* values, make them suitable for photothermal conversion of solar energy.

3.3. Electrical studies

The variation of Hall mobility, carrier density and resistivity measured at room temperature against the doping concentration is shown in Figs. 4 and 5. The values of μ, *n* and ρ are obtained from the combined measurements of resistivity and Hall coefficient. These values are comparable with the values found in literature [29,30,34]. The electrical resistivity is almost constant throughout the temperature range from 30 to 200 °C. All the samples are heavily doped and are degenerate. Film degeneracy is established by evaluating the Fermi energy by the expression

$$E_F = \left(\frac{h^2}{8m^*}\right)\left(\frac{3n}{\pi}\right)^{\frac{2}{3}} \quad (2)$$

where *h* is the Plank's constant, *n* is the concentration of free carrier and *m** is the reduced effective mass. In all the calculations a mean value of $m^* = 0.3m$ [63], where *m* is the electron rest mass, is used. The evaluated E_F values are very high compared to *kT* (~0.03 eV) at room temperature. The observed variation of μ and ρ is small in the composition ranges investigated. For both the dopants, the carrier density initially increases with increasing concentration and then decreases. The respective peak concentrations occur at the weight ratios of $[NH_4F]/[SnCl_2] = 10$ wt.% and $[SbCl_3]/[SnCl_2] = 0.6$ wt.%.

A semiconducting system may return to equilibrium after the application of an external field as a result of scattering. Free carriers may interact with a variety of scattering centres. These centres may be impurity atoms (ionised or neutral), thermal vibrations (acoustical and optical) of the lattice atoms, structural defects (dislocations, vacancies) and other obstacles. In polycrystalline thin film semiconductors, apart form the above scattering centres, the influence of the grain boundary has also to be taken into account. The interaction between the carriers and the scattering centres determines the actual value of the mobility of the carriers in these materials.

In the interpretation of the results obtained for a given transport phenomenon, one has to deal with the problem of mixed scattering of carriers. To solve this problem, one has to identify the main scattering mechanisms and then determine their contributions. The scattering also varies with the temperature and with the impurity concentration.

In analysing the mobility data of the samples, the relaxation times characteristic of the various scattering mechanisms can be added together reciprocally to give an effective relaxation time [64], if the mechanisms can be regarded as independent. The mobility μ is obtained as

$$\mu = \frac{e}{m^*}\langle\tau\rangle \quad (3)$$

With $\langle\tau\rangle$ a suitable average over the energy-dependent relaxation times. The angle brackets are omitted in the following discussion.

For the scattering by neutral impurities we have approximately [65]

$$\tau_n = \frac{(\pi\, m^*\, e)^2}{10\varepsilon\, h^3\, N_n} \quad (4)$$

where N_n the concentration of neutral impurities and ε the absolute dielectric permittivity; the other symbols have their usual meanings. For the heavy doping case, this form of scattering is unimportant because, right down to low temperatures (~77 K), impurities in heavily doped semiconductors are fully ionised.

All the doped SnO_2 films prepared here are polycrystalline. They are composed of crystallites joined together by grain boundaries, which are transitional regions between different orientations of neighbouring crystallites. These boundaries between grains play a significant

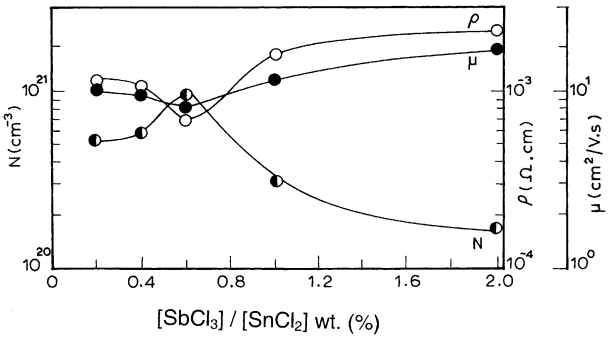

Fig. 5. Variation of Hall mobility (μ), carrier density (*N*) and resistivity (ρ) with dopant weight ratio for SnO_2:Sb thin films.

role in the scattering of charge carriers in polycrystalline thin coatings. To analyse the effects of grain boundaries on electrical properties of thin film materials two models have been employed. The first is a charge trapping model [66,67] where it is assumed that grain boundaries contain trapping states induced by lattice defects. These states compensate a fraction of the charge carriers of the ionised uniformly distributed dopants. This process creates a potential barrier across the depletion region, impeding the carrier motion from one crystallite to another. The influence of the grain size becomes very important when the depletion layer width becomes comparable with the grain size of the crystallite. The second model is a dopant segregation model. In this case the grain boundaries are assumed to act as sinks for the preferential segregation of the dopants. Therefore they become inactive in the boundary layers [68,69].

The first model has been employed to analyse the experimentally measured mobility values of the charge carriers in doped and undoped SnO_2 films [29,49]. In this model the conduction mechanism is based on thermionic emission over the potential barrier. This, of course, requires a barrier energy larger than kT. The barrier energy calculation is done by fitting the measured mobility to some functional form derived on the basis of themionic emission over intergrain barriers. As for the degenerate samples, since the mobility shows feeble variation with temperature, this model is not suitable because the activation energy is smaller than kT. This is true in the present study also, since the resistivity remains nearly constant throughout the temperature range of 30–200 °C for all the samples.

Another condition is that the mean free path l of the free carriers should be comparable to the size of the grains in the films. For the degenerate samples l can be estimated with the expression [70]

$$l = \left(\frac{h}{2e}\right)\left(\frac{3n}{\pi}\right)^{\frac{1}{3}}\mu \tag{5}$$

where n is the carrier concentration and μ is the measured mobility. The mean free path values calculated for the sample lie in the range of 14–20 Å. These l values are considerable shorter than crystallite dimensions calculated using X-ray data. Based on the above discussion it is concluded that grain boundary scattering is not the dominant mechanism. The resistivity and carrier concentration of fluorine doped SnO_2 films determined by Hall measurements at room temperature have been analysed by Bruenaux et al. [40] within the frame of the grain boundary model. The conclusion arrived at is that at large carrier densities, the influence of grain boundaries becomes negligible. Similar conclusions have been arrived by Haitijema et al. [39] in the case of fluorine doped layers with high electron concentrations. The explanation given in arriving at this conclusion is that the Fermi energy, which is proportional to $n^{2/3}$ is much higher for the doped samples. So, the free electrons in the doped samples have a much higher energy and will move easily across the inter-grain energy barriers.

Another scattering mechanism prevalent in doped semiconductors is the ionised impurity scattering. According to the Brooks–Herring formula [71], the relaxation time for coupling to ionised impurities is, in the degenerate case, given by

$$\tau_i = \frac{(2m^*)^{1/2}\,\varepsilon^2\,E_F^{3/2}}{\pi\,e^4\,N_i f(x)} \tag{6}$$

with N_i the carrier concentration of ionised impurities and $f(x)$ given by

$$f(x) = \ln(1+x) - \frac{x}{1+x} \tag{7}$$

with

$$x = \frac{8m^*\,E_F\,R_S^2}{\hbar^2} \tag{8}$$

The screening radius R_s is given by

$$R_S = \frac{\hbar}{2e}\left(\frac{\varepsilon}{m^*}\right)^{\frac{1}{2}}\left(\frac{\pi}{3N_i}\right)^{\frac{1}{6}} \tag{9}$$

where ε is the absolute dielectric permittivity and m^* is the effective mass of the carriers.

Substitution of the τ_i expression [Eq. (6)] in Eq. (3) yields the expression for mobility due to ionised impurities as

$$\mu_i = \left(\frac{2}{m^*}\right)^{\frac{1}{2}}\frac{\varepsilon^2\,E_F^{3/2}}{\pi\,e^3 f(x)\,N_i} \tag{10}$$

Since all the dopant atoms will be fully ionised at room temperature, impurity ion concentration will be equal to the free carrier concentration. Thus taking $N_i = n$ and calculating E_F with the expression given in Eq. (2), mobility values are calculated using the expression in Eq. (10).

The calculated mobility values are tabulated in Table 3 along with mean free path, carrier concentration and measured mobility values for different dopants. The calculated mobility values are comparable to the measured values. This clearly indicates that the main damping mechanism limiting the mobility in doped SnO_2 samples is the ionised impurity scattering. In addition, scattering by impurity ions predicts an increasing mobility with decreasing concentration, which is also evident from Table 3. This further supports the above conclusion.

From the foregoing discussion, it is concluded that ionised impurity scattering is the dominant mechanism in the films. Similar conclusions have been reported by other workers [2,9,27,39,43]. This conclusion means

Table 3
Comparison of observed and calculated mobility (μ) data along with carrier concentration (n) and mean free path (l) values of different dopant ratios of SnO_2 thin films

Dopant	Wt. ratio	n ($\times 10^{20}$ cm^{-3})	l (Å)	μ_{obs} (cm^2 V^{-1} s^{-1})	μ_{cal} (cm^2 V^{-1} s^{-1})
F	4	5.701	14	9.6	8.8
	6	6.800	16	9.0	8.2
	8	8.333	18	8.5	7.6
	15	10.420	15	7.5	6.9
	10	13.160	16	7.0	6.3
Sb	2	1.671	19	16.7	15.2
	1	3.102	17	12.6	11.5
	0.2	5.162	13	10.1	9.2
	0.4	5.950	17	9.6	8.7
	0.6	9.523	20	8.1	7.2
(F+Sb)	10+0.5	1.333	18	17.2	16.9
	15+0.5	1.553	18	16.1	15.7
	10+0.2	2.645	17	13.0	12.3
	12+1	4.055	18	11.6	10.2
	7.5+1	4.257	17	11.2	10.0
	8+1	5.061	16	10.0	9.3

that the conductivity σ is mainly determined by the free carrier concentration in these films, because mobility and carrier concentrations are no longer independent of each other.

Further effort is under progress to decrease the film thickness and increase the optical transmission without increasing the sheet resistance. This combination is needed for the usage of transparent conducting window material in thin film solar cells.

4. Conclusion

Transparent conducting doped SnO_2 layers have been prepared by spray pyrolysis from $SnCl_2$ precursor solution. Structural and electrical properties of the films have been analysed for three cases of doping: fluorine, antimony, and (F+Sb). Structural investigations using XRD reveal that the layers are composed of SnO_2 only. No other phases are detected. The lattice parameter values are not affected by the doping. The preferred orientation is in (200) direction and the grain sizes are independent of the dopant. The average grain size is approximately 300 Å. The lowest sheet resistance of 5.65 $\Omega/\square$ is obtained for the SnO_2:F film. Better transparency is achieved with fluorine doping. Moderately high figure-of-merit values are obtained for $\sim$1-μm-thick fluorine doped samples. All the films are degenerate with carrier concentrations in the range of 1.3×10^{20}–1.3×10^{21} cm^{-3}. The resistivities of the samples are of the order of 10^{-3}–10^{-4} Ω-cm. Fluorine doped samples are having lower mobility than the antimony and (F+Sb) doped samples. From the electrical investigations it is concluded that the ionised impurity scattering is the dominant mechanism limiting the mobility of the samples. The carrier concentration determines the resistivity of the films.

Acknowledgements

The author is gratefully acknowledged to Prof E.S.R. Gopal and Dr K.S. Sanguuni, Department of Physics, Indian Institute of Science; Prof M. Laxmanan and Dr K. Ramamurthi, Department of Physics, Prof C. Thangamuthu, Department of Economics, Bharathidasan University and Prof A. Srinivasan, Department of Physics, Indian Institute of Technology, Guwahati, for their help, moral support and encouragement, when I had difficulties during the course of this work. The author sincerely thanks to the referee's valuable suggestions to improve the quality and clarity of the manuscript. The Department of Physics, Sri Venkateswara University, Tirupathi, and the Inter University Consortium, Indore, are acknowledged sincerely for the usage of Hall set-up and for recording the XRD spectra, respectively. The author would like to thank Dr R. Arvinda Narayanan and S. Jaisankar, for their critical reading of the manuscript.

References

[1] A. Goetzberger, C. Hebling, Sol. Energy Mater. Sol. Cells 62 (2000) 1.
[2] G. Frank, E. Kaur, H. Kostlin, Sol. Energy Mater. 8 (1983) 387.
[3] S. Cohen, Thin Solid Films 77 (1981) 127.
[4] W.Y. Chung, C.H. Shim, S.D. Choi, D.D. Lee, Sens. Act. B 20 (1994) 139.

[5] J.R. Brown, P.W. Haycock, L.M. Smith, A.C. Jones, E.W. Williams, Sens. Act. B 63 (2000) 109.
[6] P. Nelli, G. Faglia, G. Sberveglieri, E. Cereda, G. Gabetta, A. Dieguez, A.R. Rodriguez, J.R. Morante, Thin Solid Films 371 (2000) 249.
[7] I. Stambolova, K. Konstantinov, Ts. Tsacheva, Mater. Chem. Phys. 63 (2000) 177.
[8] R. Gomer, Rev. Sci. Instrum. 24 (1953) 993.
[9] Z.M. Jarzebski, J.P. Marton, J. Electrochem. Soc. 123 (1976) 199C; 299C; 333C.
[10] J.L. Vossen, Phys. Thin Films 9 (1977) 1.
[11] G. Haacke, Annu. Rev. Mater. Sci. 7 (1977) 73.
[12] K.L. Chopra, S. Major, D.K. Pandya, Thin Solid Films 102 (1983) 1.
[13] A.L. Dawar, J.C. Joshi, J. Mater. Sci. 19 (1984) 1.
[14] P.S. Patil, Mater. Chem. Phys. 59 (1999) 185.
[15] A. Czapla, E. Kusior, M. Bucko, Thin Solid Films 182 (1989) 15.
[16] T. Pisarkiewicz, T. Stapinski, Thin Solid Films 174 (1989) 277.
[17] F.C. Stedile, B.A.S. De Barros, B. Leite, F.L. Freire, R. Baumvol, W.H. Schreiner, Thin Solid Films 170 (1989) 285.
[18] B.P. Howson, H. Barankova, A.G. Spencer, Thin Solid Films 196 (1991) 315.
[19] R.S. Dale, C.S. Rastomjee, F.H. Potter, R.G. Egdell, J. Tate, Appl. Surf. Sci. 70/71 (1993) 359.
[20] Y. Watanabe, H. Endo, H. Semba, M. Takata, J. Non-Cryst. Solids 178 (1994) 84.
[21] Y. Onuma, Z. Wang, H. Ito, M. Nakao, K. Kamimura, Jpn. J. Appl. Phys. 37 (1998) 963.
[22] M. Ruske, G. Brauer, J. Szczyrbowski, Thin Solid Films 351 (1999) 146.
[23] D. Belanger, J.P. Dodelet, B.A. Lombos, J.I. Dickson, J. Electrochem. Soc. 132 (1985) 1398.
[24] A.C. Arias, L.S. Roman, T. Kugler, R. Toniolo, M.S. Meruvia, I.A. Hummelgen, Thin Solid Films 371 (2000) 29.
[25] O.K. Varghese, L.K. Malhotra, J. Appl. Phys. 87 (2000) 7457.
[26] M.K. Karanjai, D.D. Gupta, J. Phys. D: Appl. Phys. 21 (1988) 356.
[27] T. Arai, J. Phys. Soc. Jpn. 15 (1960) 916.
[28] S. Kulaszewicz, I. Lasocka, C.Z. Michalski, This Solid Films 55 (1978) 283.
[29] E. Shanthi, V. Dutta, A. Banerjee, K.L. Chopra, J. Appl. Phys. 51 (1980) 6243.
[30] E. Shanthi, A. Banerjee, V. Dutta, K.L. Chopra, J. Appl. Phys. 53 (1982) 1615.
[31] E. Shanthi, A. Banerjee, K.L. Chopra, Thin Solid Films 88 (1982) 93.
[32] P. Grosse, F.J. Schmitte, Thin Solid Films 90 (1982) 309.
[33] G. Mavrodiev, M. Gajdardziska, N. Novkovski, Thin Solid Films 113 (1984) 93.
[34] J.J.Ph. Elich, E.C. Boslooper, H. Haitjema, Thin Solid Films 177 (1989) 17.
[35] M. Fantini, I. Torriani, Thin Solid Films 138 (1986) 255.
[36] S.P.S. Arya, Cryst. Res. Technol. 21 (1986) 3.
[37] C. Agashe, M.G. Takwale, B.R. Marathe, V.G. Bhide, Sol. Energy Mater. 17 (1988) 99.
[38] A.I. Onyia, C.E. Okeke, J. Phys. D: Appl. Phys. 22 (1989) 1515.
[39] H. Haitjema, J.J.Ph. Elich, C.J. Hoogendoorn, Sol. Energy Mater. 18 (1989) 283.
[40] J. Bruneaux, H. Cachet, M. Froment, A. Messad, Thin Solid Films 197 (1991) 129.
[41] M. Kojima, H. Kato, M. Gatto, Philos. Mag. B 68 (1993) 215.
[42] G. Gordillo, L.C. Moreno, W. de la Cruz, P. Teheran, Thin Solid Films 252 (1994) 61.
[43] C. Agashe, S.S. Major, J. Mater. Sci. 31 (1996) 2965.
[44] D.R. Acosta, E.P. Zironi, E. Montoya, W. Estrada, Thin Solid Films 288 (1996) 1.
[45] A. Malik, A. Seco, E. Fortunato, R. Martin, J. Non-Cryst. Solids 227–230 (1998) 1092.
[46] Q. Chen, Y. Qian, Z. Chen, G. Zhou, Y. Zhang, Thin Solid Films 264 (1995) 25.
[47] A. Smith, J.M. Laurent, D.S. Smith, J.P. Bonnet, R.R. Clemente, Thin Solid Films 266 (1995) 20.
[48] K. Omura, P. Veluchamy, M. Murozono, J. Electrochem. Soc. 146 (1999) 2113.
[49] K.L. Chopra, R.C. Kainthla, D.K. Pandya, A.P. Thakoor, Phys. Thin Films 12 (1982) 167.
[50] K. Nomura, Y. Ujihira, S.S. Sharma, A. Fueda, T. Murakami, J. Mater. Sci. 24 (1989) 937.
[51] B. Thangaraju, P. Kaliannan, Cryst. Res. Technol. 35 (2000) 71.
[52] B. Thangaraju, P. Kaliannan, J. Phys. D: Appl. Phys. 33 (2000) 1054.
[53] B. Thangaraju, P. Kaliannan, Semicond. Sci. Technol. 15 (2000) 542.
[54] B. Thangaraju, P. Kaliannan, Semicond. Sci. Technol. 15 (2000) 849.
[55] A.E. Rakhshani, Y. Makdisi, H.A. Ramazaniyan, J. Appl. Phys. 83 (1998) 1049.
[56] L.J. van der Pauw, Philips Res. Rep. 13 (1958) 1.
[57] B. Thangaraju, Some Investigations on Spray Deposited Thin Films of Oxides and Chalcogenides of Lead and Tin, Ph.D Thesis, Bharathidasan University, Trichy, India (unpublished), 1999, pp. 36–37.
[58] M. Hecq, A. Dubois, J. Van Cakenberghe, Thin Solid Films 18 (1973) 117.
[59] N.S. Murthy, S.R. Jawalekar, Thin Solid Films 100 (1983) 219.
[60] Gmelin, Hanbuch der Anorganische Chemie — Tin Part C5, Springer-Verlag, New York, 1977, p. 68.
[61] P. Pascal, Nouveau Traite de Chimie Minerale, vol. 8, Masson, Paris, France, 1963, pp. 313, 369.
[62] G. Haacke, J. Appl. Phys. 47 (1976) 4086.
[63] H. Haitjema, J.J.Ph. Elich, Sol. Energy Mater. 16 (1987) 79.
[64] F.J. Blatt, Physics of Electronic Conduction in Solids, McGraw Hill, New York, 1968, p. 59.
[65] C. Erginsoy, Phys. Rev. 79 (1950) 1013.
[66] T.I. Kamins, J. Appl. Phys. 42 (1971) 4357.
[67] J.Y.W. Seto, J. Appl. Phys. 46 (1975) 5247.
[68] M.E. Cowher, T.O. Sedgwick, J. Electrochem. Soc. 119 (1972) 1565.
[69] B.A. Lombos, S. Yee, M. Pietrantonio, M. Averous, J. Phys. 43 (1982) C1–C199.
[70] S. Noguchi, H. Sakata, J. Phys. D: Appl. Phys. 13 (1980) 1129.
[71] V.I. Fistul, Heavily Doped Semiconductors, Plenum Press, New York, 1969, p. 86.